Measurements of the BK_{Ca} Channel's High-Affinity Ca^{2+} Binding Constants: Effects of Membrane Voltage

Tara-Beth Sweet and Daniel H. Cox

Molecular Cardiology Research Institute, Tufts Medical Center, and The Department of Neuroscience, Tufts University School of Medicine, Boston, MA 02111

It has been established that the large conductance Ca^{2+}-activated K^+ channel contains two types of high-affinity Ca^{2+} binding sites, termed the Ca^{2+} bowl and the RCK1 site. The affinities of these sites, and how they change as the channel opens, is still a subject of some debate. Previous estimates of these affinities have relied on fitting a series of conductance–voltage relations determined over a series of Ca^{2+} concentrations with models of channel gating that include both voltage sensing and Ca^{2+} binding. This approach requires that some model of voltage sensing be chosen, and differences in the choice of voltage-sensing model may underlie the different estimates that have been produced. Here, to better determine these affinities we have measured Ca^{2+} dose–response curves of channel activity at constant voltage for the wild-type mSlo channel (minus its low-affinity Ca^{2+} binding site) and for channels that have had one or the other Ca^{2+} binding site disabled via mutation. To accurately determine these dose–response curves we have used a series of 22 Ca^{2+} concentrations, and we have used unitary current recordings, coupled with changes in channel expression level, to measure open probability over five orders of magnitude. Our results indicate that at −80 mV the Ca^{2+} bowl has higher affinity for Ca^{2+} than does the RCK1 site in both the opened and closed conformations of the channel, and that the binding of Ca^{2+} to the RCK1 site is voltage dependent, whereas at the Ca^{2+} bowl it is not.

INTRODUCTION

Large-conductance Ca^{2+}-activated potassium (BK_{Ca}) channels are important for the modulation of many physiological processes, such as neuronal firing, smooth muscle contraction, and neurotransmitter release (Storm, 1987; Roberts et al., 1990; Sah and McLachlan, 1992; Robitaille et al., 1993; Nelson and Quayle, 1995; Brenner et al., 2000; Hu et al., 2001; Wang et al., 2001; Semenov et al., 2006). They are uniquely suited to regulate these processes because they are sensitive to both intracellular Ca^{2+} and membrane voltage. This is seen as a leftward shift in the BK_{Ca} channel's conductance–voltage (G-V) relation as the internal Ca^{2+} concentration is increased. Biophysical studies have shed considerable light on the mechanisms by which voltage influences channel opening (Cui et al., 1997; Stefani et al., 1997; Diaz et al., 1998; Horrigan and Aldrich, 1999, 2002; Horrigan et al., 1999; Rothberg and Magleby, 2000; Bao and Cox, 2005); however, the mechanisms by which Ca^{2+} influences channel opening remain less well understood.

Unlike K^+ channels gated solely by voltage, the BK_{Ca} channel's pore-forming α subunit (four per functional channel) contains a large intracellular domain that confers Ca^{2+} sensitivity on a voltage-gated structure (Wei et al., 1994; Schreiber and Salkoff, 1997; Schreiber et al., 1999). The structure of this domain remains a matter of debate; however, it is generally agreed that within this domain there are three distinct Ca^{2+} binding sites, one of low affinity (millimolar dissociation constants) and two of high affinity (micromolar dissociation constants) (Bao et al., 2002; Shi et al., 2002; Xia et al., 2002; Magleby, 2003). Mutations at these sites together eliminate the BK_{Ca} channel's characteristic Ca^{2+}-dependent G-V shift (Xia et al., 2002). The first of these sites to be identified, the Ca^{2+} bowl, is an aspartate-rich region near the carboxy terminus (Schreiber and Salkoff, 1997). Considered high affinity, this site contributes to the channel's Ca^{2+} sensitivity in the micromolar range (Bao et al., 2002; Xia et al., 2002). Mutations within the Ca^{2+} bowl such as D897-901N (referred to as D5N5) or D898A/D900A (referred to here as D2A2) can eliminate the contribution of this site to the channel's Ca^{2+} sensitivity (Bian et al., 2001; Bao et al., 2004). The second high-affinity site, termed here the RCK1 site, resides in a domain thought to be similar in structure to the ligand binding RCK domains of bacterial potassium channels and transporters (Schreiber and Salkoff, 1997; Jiang et al., 2001; Bao et al., 2002; Jiang et al., 2002; Xia et al., 2002;

Correspondence to Daniel H. Cox: dan.cox@tufts.edu

Abbreviations used in this paper: BK_{Ca} channel, large-conductance Ca^{2+}-activated potassium channel; G-V, conductance–voltage; mSlo, mouse Slo.

The online version of this article contains supplemental material.

The Rockefeller University Press $30.00
J. Gen. Physiol. Vol. 132 No. 5 491–505
www.jgp.org/cgi/doi/10.1085/jgp.200810094

Zeng et al., 2005). Although the residues that coordinate Ca^{2+} at this site have yet to be determined, the mutation D367A has been shown to eliminate the contribution of this second high-affinity site to Ca^{2+} sensing (Xia et al., 2002). The BK_{Ca} channel's low-affinity Ca^{2+} binding site is also thought to reside in the channel's RCK1 domain, and its influence can be eliminated by the mutation E399N (Shi et al., 2002; Xia et al., 2002).

The binding properties of the BK_{Ca} channel's two high-affinity Ca^{2+} binding sites are uncertain. Bao et al. (2002) estimated the Ca^{2+} bowl's Ca^{2+} dissociation constant to be 3.5 μM when the channel is closed (K_C) and 0.8 μM when it is open (K_O) (Bao et al., 2002), whereas Xia et al. (2002) estimated K_C to be 4.5 μM and K_O to be 2.0 μM (Xia et al., 2002). These numbers may seem similar, but according to allosteric theory the ratio K_C/K_O is equivalent to the factor by which Ca^{2+} binding at a given site alters the equilibrium constant for channel opening. The estimates of Bao et al. (2002) yield a K_C/K_O value of 4.4, whereas those of Xia et al. (2002) yield a K_C/K_O value of 2.2. Thus, for a single binding event the two groups predict effects of Ca^{2+} on the equilibrium constant for channel opening that differ by a factor of two, and if there are four Ca^{2+} bowl–related sites—as there appears to be (Niu and Magleby, 2002)—then when all four sites are occupied, the difference is 14-fold. Further, there are larger differences between the two groups' estimates of K_C and K_O for the channel's other type of high-affinity Ca^{2+} binding site, the RCK1 site. The estimates of Bao et al. (2002) are considerably smaller than those of Xia et al. (2002) and more like those of the Ca^{2+} bowl (Bao et al. [2002]: K_C = 3.8 μM and K_O = 0.9 μM; Xia et al. [2002]: K_C = 17.2 μM and K_O = 4.6 μM).

One likely reason for these discrepancies is that both groups made their estimates by fitting gating models to a series of G-V relations determined for a series of $[Ca^{2+}]$, and to make these estimates they necessarily had to assume some model of the voltage-sensing mechanism of the channel. The two groups used different voltage-sensing models. More generally, however, a better way to estimate the affinity constants of the channel's Ca^{2+} binding sites would be to study the effect of Ca^{2+} on channel opening at many $[Ca^{2+}]$ but at a single voltage, such that the effect of voltage on channel opening can be treated as a constant.

Here, we have taken this approach. We have used mutations at each type of Ca^{2+} binding site and high-resolution Ca^{2+} dose-response curves to characterize the binding properties of each of the BK_{Ca} channel's high-affinity Ca^{2+} binding sites at both −80 and 0 mV. Our results indicate that the two sites have substantially different affinities, as suggested by Xia et al. (2002), at both these potentials, and that Ca^{2+} binding at the RCK1 site is voltage dependent, whereas at the Ca^{2+} bowl it is not.

MATERIALS AND METHODS

Heterologous Expression of BK_{Ca} Channels in TSA 201 Cells

TSA201 cells (modified human embryonic kidney cells) were transiently transfected with expression vectors (pcDNA 3; Invitrogen) encoding the α subunit of the BK_{Ca} channel from mouse (mSlo-mbr5) (Butler et al., 1993), enhanced green fluorescent protein (eGFP-N1; BD Biosciences), and the empty pcDNA 3.1+ vector (Invitrogen) to control for total amount of transfected DNA. Cells were transiently transfected using the Lipofectamine 2000 reagent (Invitrogen). The enhanced green fluorescent protein was used to monitor successfully transfected cells. For transfection, cells at 80–90% confluence in 35-mm falcon dishes were incubated with a mixture of the plasmids (total of 4 μg DNA) Lipofectamine and Optimem (Invitrogen) according to the manufacturer's instructions. In brief, the mixture was left on the cells 4–8 h after which the cells were replated into recording Falcon 3004 dishes in standard tissue culture media: DMEM with 1% fetal bovine serum, 1% L-glutamine, and 1% penicillin-streptomycin solution (all from Invitrogen). The cells were patch-clamped 1–3 d after transfection.

Electrophysiology

All recordings were performed in the inside-out patch-clamp configuration (Hamill et al., 1981). Patch pipettes were made of borosilicate glass (VWR micropipettes) with 0.8–5-MΩ resistances that were varied for different recording purposes. The tips of the patch pipettes were coated with sticky wax (KerrLab) and fire polished. Data were acquired using an Axopatch 200B patch clamp amplifier and a Macintosh-based computer system equipped with an ITC-16 hardware interface (InstruTECH) and Pulse acquistion software (HEKA electronik). For macroscopic current recordings, data were sampled at 50 kHz and filtered at 10 kHz. In most macroscopic current recordings, capacity and leak current were subtracted using a P/5 subtraction protocol with a holding potential of −120 mV and leak pulses in opposite polarity to the test pulse, but with BK_{Ca} currents recorded with >100 μM Ca^{2+}, no leak subtraction was performed.

Unitary current recordings acquired at −80 mV were sampled at 100 KHz and filtered at 10 KHz. Unitary current recordings acquired at 0 mV were sampled at 100 kHz and filtered at 2 kHz. All experiments were performed at room temperature, 22–24°C.

Solutions

The pipette solution for macroscopic current recordings contained the following: 118 mM $KMeSO_3$, 20 mM *N*-methyl-glucamine-$MeSO_3$, 2 mM KCl, 2 mM $MgCl_2$, 2 mM HEPES, pH 7.20. The pipette solution for current recordings at 0 mV contained the following: 3 mM $KMeSO_3$, 135 mM *N*-methyl-glucamine-$MeSO_4$, 2 mM KCl, 2 mM $MgCl_2$, 2 mM HEPES, pH 7.20. 10 μM $GdCl_3$ was added to both pipette solutions to block endogenous stretch-activated channels. $GdCl_3$ did not block BK_{Ca} currents (not depicted) (Yang and Sachs, 1989; Qian and Magleby, 2003). The bath solution for all recordings contained the following: 118 mM $KMeSO_3$, 20 mM *N*-methyl-glucamine-$MeSO_3$, 2 mM KCl, 2 mM HEPES, pH 7.20. 1 mM EGTA (Fluka) was used as the Ca^{2+} buffer for solutions containing 3–500 nM free $[Ca^{2+}]$. 1 mM HEDTA (Sigma-Aldrich) was used as the Ca^{2+} buffer for solutions containing 0.8–20 μM free $[Ca^{2+}]$, and no Ca^{2+} chelator was used in solutions containing between 20 μM and 2.5 mM free Ca^{2+}. 50 μM (+)-18-crown-6-tetracarboxylic acid (18C6TA) was added to all internal solutions to prevent contaminant Ba^{2+} block at high voltages. Both internal and external solutions were brought to pH 7.20.

The appropriate amount of total Ca^{2+} (100 mM $CaCl_2$ standard solution; Orion Research, Inc.) to add to the buffered solutions to yield the desired approximate free Ca^{2+} concentrations of 3 nM to 2.5 mM was calculated using the program MaxChelator (see Online Supplemental Material), and the solutions were prepared as described previously (Bao et al., 2002). The Ca^{2+} concentrations reported are averages of three independent measurements determined with an Orion Ca^{2+}-sensitive electrode. The solutions bathing the intracellular side of the patch were changed by means of a DAD valve–controlled pressurized superfusion system (ALA Scientific Instruments).

Data Analysis

All data analysis was performed with Igor Pro graphing and curve-fitting software (WaveMetrics Inc.), and the Levenberg-Marquardt algorithm was used to perform nonlinear least-square curve fitting. Values in the text are given ± SEM.

G-V Curves

G-V relations were determined from the amplitude of tail currents measured 200 μs after repolarizations to −80 mV following voltage steps to the test voltage. Each G-V relation was fitted with a Boltzmann function,

$$G = \frac{G_{\max}}{1 + e^{\frac{-zF(V - V_{1/2})}{RT}}},$$

and normalized to the maximum of the fit.

Single-Channel Analysis

Under conditions where the open probability (*Popen*) is small ($<10^{-2}$), single-channel openings were observed in patches containing hundreds of channels and I_K was measured from steady-state recordings 30 s in duration. *NPopen* was determined from all-points histograms by measuring the fraction of time spent (P_K) at each open level (k) using a half-amplitude criteria and summing their contributions, $NPopen = \Sigma\, kP_K$, where N is the number of channels in the patch.

Popen Versus Ca^{2+} Curves

The effect of Ca^{2+} on *Popen* was determined from the ratio of *NPopen* at a given Ca^{2+} to *NPopen* at 5.3 μM Ca^{2+} for all Ca^{2+} concentrations tested on a given patch. The ($NPopen/NPopen_{5.3\ \mu M}$) versus [$Ca^{2+}$] relation from each patch was then plotted and averaged across many patches. The mean ($NPopen/NPopen_{5.3\ \mu M}$) versus [$Ca^{2+}$] relation was then adjusted such that at 3 nM Ca^{2+} log ($NPopen/NPopen_{min}$) = 0. In some cases *Popen*, rather than being normalized ($NPopen/NPopen_{min}$), was reported as a function of [Ca^{2+}]. This was done by determining *Popen* for each channel type at a single [Ca^{2+}] in separate experiments, and then adjusting the average log ($NPopen/NPopen_{min}$) versus log [Ca^{2+}] curve vertically, such that *Popen* was correct at the [Ca^{2+}] at which *Popen* was known. At 0 mV, the calibrated *Popen* was determined at 2.5 mM from patches whose channel content was apparent (n = 1–4). At −80 mV, the calibrating *Popen* was determined at 5.3 μM [Ca^{2+}] from unitary current measurements of *NPopen* from a series of patches in which N was calculated from the maximal current measured at +80 mV and separate *Popen* measurements taken at +80 mV for single channels.

Online Supplemental Material

The amount of Ca^{2+} to add to internal solutions to yield the desired free Ca^{2+} concentrations was calculated using the program MaxChelator, which was downloaded from http://www.stanford.edu/~cpatton/maxc.html and is included as executable files here. The online supplemental material is available at http://www.jgp.org/cgi/content/full/jgp.200810094/DC1.

RESULTS

The Effect of Ca^{2+} with Both Sites Intact

The BK_{Ca} channel is both Ca^{2+} and voltage sensitive, and the effects of these stimuli are often displayed as a series of G-V relations determined at several Ca^{2+} concentrations (Barrett et al., 1982). Such a series, determined from BK_{Ca} channels exogenously expressed in TSA-201 cells, is shown in Fig. 1 B. The data are from excised inside-out macropatches (Fig. 1 A). Increasing intracellular Ca^{2+} shifts the channel's G-V curve leftward, an effect that is known under wild-type conditions to be due to three types of Ca^{2+} binding sites, two of high affinity and one of low affinity. The channels in the patches of Fig. 1, however, contained the mutation E399N, which eliminates low-affinity Ca^{2+} sensing (Shi et al., 2002; Xia et al., 2002) and thereby allows one to examine high-affinity Ca^{2+} sensing in isolation. We refer to the mouse Slo (mSlo) channel carrying this mutation as ΔE. Increasing Ca^{2+} from 3 nM to 2.5 mM shifts the ΔE G-V relation $\backsim$−200 mV.

Previous estimates of the affinities of the BK_{Ca} channel's high-affinity Ca^{2+} binding sites have been based on fitting gating models to data like that shown in Fig. 1 B. This necessarily requires that one assume some model of voltage-dependent gating, and the resulting Ca^{2+} binding parameters produced by the fits are then dependent on this choice (Bao et al., 2002; Xia et al., 2002). To circumvent this necessity, and thereby more directly determine the BK_{Ca} channel's high-affinity Ca^{2+} binding constants, here we have studied the effects of Ca^{2+} at constant voltage.

Fig. 2 A shows unitary ΔE currents recorded from a single membrane patch at −80 mV and four different [Ca^{2+}]. Corresponding amplitude histograms are shown in Fig. 2 B. Although the patch contained hundreds of channels, each channel's open probability (*Popen*) is low in the absence of Ca^{2+}, such that activity is observed as the infrequent and brief opening of single channels. Application of Ca^{2+} then caused a large increase in *Popen* that resulted in multi-channel openings. From data like these we derived the ΔE channel's *Popen* versus [Ca^{2+}] relation (Fig. 2 C). So that all parts of the curve could be well determined, *Popen* was measured over five orders of magnitude with 22 Ca^{2+} concentrations. To do this, many patches were used and normalized by their values of *NPopen* at 5.3 μM, where N is the number of channels in a given patch. The data were then averaged at each [Ca^{2+}], and the whole curve was adjusted vertically to match the BK_{Ca} channel's *Popen* at 5.3 μM and −80 mV, which was determined in separate experiments (see Materials and methods).

These data were then analyzed as follows. If one assumes that there are four of each type of Ca^{2+} binding site and that each site influences channel opening by altering the equilibrium constant of a single conformational

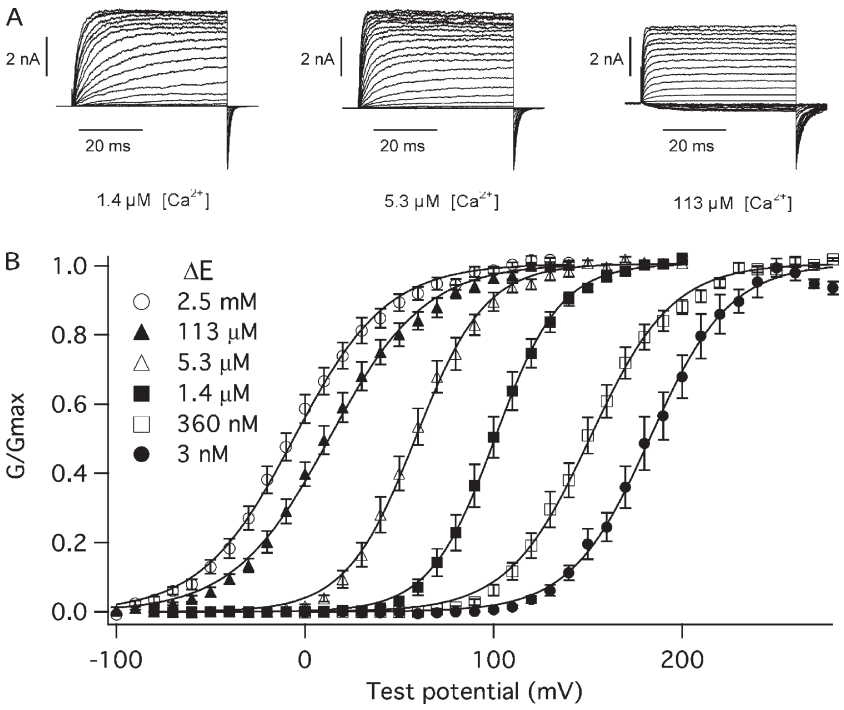

Figure 1. Macroscopic currents and normalized conductance versus voltage curves (G-V) determined for the mSlo mutant E399N (ΔE). (A) Shown are averaged macroscopic current families. Each family displayed is the average of three consecutive families recorded from a single TSA 201 inside-out macropatch exposed to 1.4, 5.3, and 113 μM [Ca^{2+}]. Membrane voltages were as follows: For 1.4 μM [Ca^{2+}] and 5.3 μM [Ca^{2+}], V_H was −80 mV, test potentials were to between −80 and +200 mV, and tail potentials were −80 mV; for 113 μM [Ca^{2+}], V_H was −150 mV, test potentials were to between −100 and +150 mV in 10-mV steps, and tail potentials were −80 mV. (B) G-V relations were determined from data like that in A at the following [Ca^{2+}]: 0.003, 0.36, 1.4, 5.3, 113, and 2,500 μM. Each curve represents the average between 7 and 13 individual curves. Error bars indicate SEM. The data have been fitted (solid lines) with a Boltzmann function ($G/G_{max} = 1/(1+e^{-qF(V-V_{1/2})/RT})$). The Boltzmann fits have the following parameters: 3 nM Ca^{2+}: Q = 1.21 *e*, $V_{1/2}$ = 183 mV; 360 nM Ca^{2+}: Q = 1.18 *e*, $V_{1/2}$ = 151 mV; 1.4 μM Ca^{2+}: Q = 1.47 *e*, $V_{1/2}$ = 101 mV; 5.3 μM Ca^{2+}: Q = 1.38 *e*, $V_{1/2}$ = 59 mV; 113 μM Ca^{2+}: Q = 1.00 *e*, $V_{1/2}$ = 13 mV; 2.5 mM Ca^{2+}: Q = 1.04 *e*, $V_{1/2}$ = –5.7 mV.

change between closed and open—as much evidence suggests (McManus and Magleby, 1991; Cox et al., 1997; Cui et al., 1997; Horrigan and Aldrich, 1999, 2002; Horrigan et al., 1999; Rothberg and Magleby, 1999, 2000; Cox and Aldrich, 2000)—and that there are no interactions between binding sites, then at constant voltage the channel's open probability as a function of voltage can be written as:

$$Popen = \frac{M(1+[Ca]/K_{O1})^4(1+[Ca]/K_{O2})^4}{(1+[Ca]/K_{C1})^4(1+[Ca]/K_{C2})^4 + M(1+[Ca]/K_{O1})^4(1+[Ca]/K_{O2})^4}, \quad (1)$$

where K_{C1} and K_{C2} represent the dissociation constants of binding sites 1 and 2 in the closed conformation. K_{O1} and K_{O2} represent the dissociation constants of binding sites 1 and 2 in the open conformation, and M represents the closed-to-open equilibrium constant when no Ca^{2+} is bound. As relates to the BK_{Ca} channel, M is voltage dependent and incorporates all effects of voltage on opening.

In the absence of Ca^{2+}, Eq. 1 reduces to:

$$Popen = \frac{M}{1+M}, \quad (2)$$

which can be rearranged to:

$$M = \frac{Popen}{1-Popen}. \quad (3)$$

Thus, M can be determined directly from *Popen* in the absence of Ca^{2+}. From Fig. 2 C we can estimate M to be $\sim 2.5 \times 10^{-6}$. However, better still, when *Popen* is small over the entire Ca^{2+} dose-response curve, as is the case here, Eq. 1 reduces to Eq. 4 below (Horrigan and Aldrich, 2002):

$$Popen \approx \frac{M(1+[Ca]/K_{O1})^4(1+[Ca]/K_{O2})^4}{(1+[Ca]/K_{C1})^4(1+[Ca]/K_{C2})^4}, \quad (4)$$

and then dividing through by *Popen* at 0 [Ca^{2+}] yields:

$$\frac{Popen(Ca)}{Popen(0)} \approx \frac{(1+[Ca]/K_{O1})^4(1+[Ca]/K_{O2})^4}{(1+[Ca]/K_{C1})^4(1+[Ca]/K_{C2})^4}. \quad (5)$$

This eliminates M and leaves a curve whose properties are determined solely by the channel's Ca^{2+} binding constants (Horrigan and Aldrich, 2002). Thus, the curve in Fig. 2 C was normalized by its minimum value to yield a *Popen* (Ca^{2+})/*Popen* (0) versus [Ca^{2+}] curve (Fig. 3) and then fitted with Eq. 5. Properties of this curve of note are: (1) Ca^{2+} increases *Popen* by a factor of 2.8×10^4; (2) *Popen* saturates at high [Ca^{2+}], ~100 μM; and (3) the curve has a shallow quality suggestive of multiple binding sites with differing affinities. Indeed the fit (solid line) yielded the following dissociation constants: SITE 1, K_{C1} = 3.7 ± 2.1 μM, K_{O1} = 0.7 ± 0.14 μM; SITE 2, K_{C2} = 51 ± 42 μM, K_{O2} = 21 ± 24 μM.

Further, when we forced both types of binding sites to have the same affinities, a substantially worse fit was obtained (dashed line, K_C = 6.1 ± 0.4 μM; K_O = 1.9 ± 0.31 μM). Thus, this analysis suggests that one of the BK_{Ca} channel's high-affinity Ca^{2+} binding sites has substantially higher

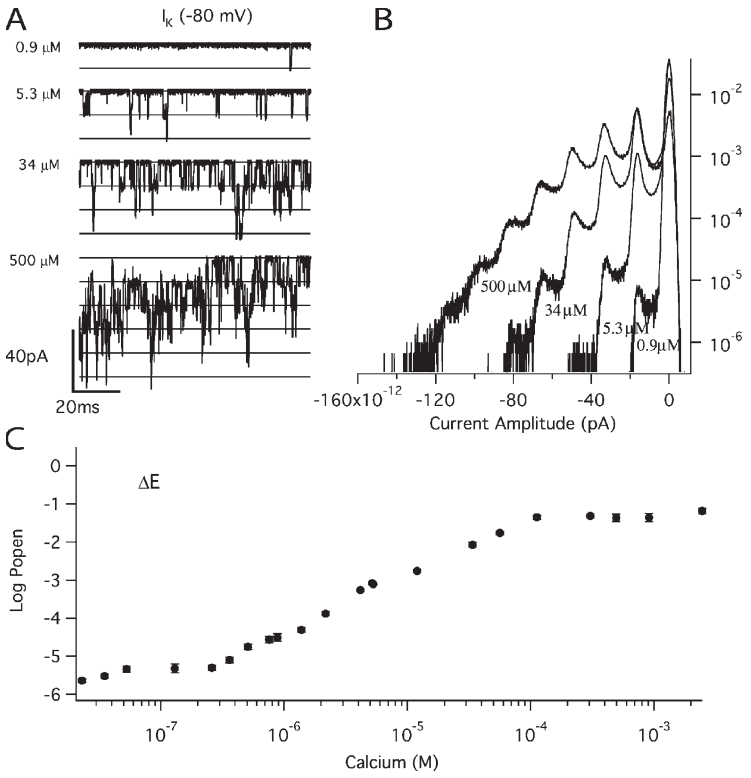

Figure 2. The Ca^{2+} dependence of *Popen* for mutant ΔE. (A) Inward potassium currents recorded at −80 mV and filtered at 10 kHz from a macropatch exposed to the indicated [Ca^{2+}] demonstrate that *Popen* increases in a Ca^{2+}-dependent manner when voltage is constant. The corresponding all-points amplitude histograms are plotted in B on a semi-log scale and were constructed from 30-s recordings at each [Ca^{2+}]. The dose–response relation for the effect of Ca^{2+} on *Popen* at negative voltage (−80 mV) is shown in C. For determination of *Popen* see Materials and methods. Each point represents the average of between 7 and 17 patches at each Ca^{2+} concentration tested. Error bars represent SEM.

affinity for Ca^{2+} than the other, both in the open and closed conformations, although noise in the data introduces some uncertainty about the fitted values.

Mutations That Eliminate Ca^{2+} Sensing

To measure the affinities of each type of high-affinity Ca^{2+} binding site individually, we used mutations that selectively eliminate the effect of Ca^{2+} at each type of site. D367A eliminates Ca^{2+} sensing via RCK1 sites (Xia et al., 2002), and D897N/D898N/D899N/D900N/D901N (D5N5) or D898A/D900A (D2A2) eliminate Ca^{2+} sensing via the Ca^{2+} bowls (Schreiber and Salkoff, 1997; Bian et al., 2001; Bao et al., 2004). Before using these mutations, however, it was important to confirm that in conjunction with E399N they eliminate all Ca^{2+} sensing. Shown in Fig. 4 A are currents recorded at various [Ca^{2+}] from a patch expressing the triple mutant (E399N) (D367A) (D897N/D898N/D899N/D900N/D901N), which we refer to as $\Delta E\Delta R\Delta B_{(D5N5)}$. Corresponding amplitude histograms are superimposed in Fig. 4 B, and in Fig. 4 C the $\Delta E\Delta R\Delta B_{(D5N5)}$ channel's Ca^{2+} dose-response relation is plotted at −80 mV. As is evident, the triple mutant shows virtually no response to Ca^{2+}, which demonstrates that the three sites targeted by these mutations can together account for all of the channel's Ca^{2+} sensing.

Ca^{2+} Binding at the Ca^{2+} Bowl

We then used the mutant (E399N) (D367A), which we refer to as ΔEΔR, to examine Ca^{2+} sensing via the Ca^{2+} bowl. Fig. 5 A compares BK_{Ca} currents at various [Ca^{2+}] recorded from a single ΔEΔR patch at −80 mV. The corresponding amplitude histograms are shown in Fig. 5 B. As with ΔE, *Popen* is low in the absence of Ca^{2+}, and activity is observed as the infrequent and brief opening of single channels. Application of Ca^{2+} then increases *Popen*, but the increase is not as great (∼10^2-fold) as it is with the ΔE channel (∼10^4-fold), presumably because the ΔEΔR channel has lost half of its high-affinity binding sites. A Ca^{2+} dose–response relation for the ΔEΔR channel at −80 mV is shown in Fig. 5 C. The affinities of

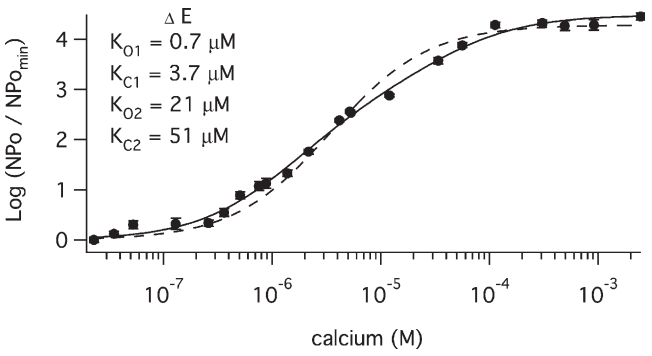

Figure 3. The Ca^{2+} binding affinity of mutant ΔE at −80 mV. The mean log ratio of N*Popen* in the presence and absence of Ca^{2+} determined from the data shown in Fig. 2. Log (N*Popen* / N$Popen_{min}$) spans the entire [Ca^{2+}] range and is fit (solid line) by Eq. 5 yielding values of K_{O1} = 0.7 μM, K_{C1} = 3.7 μM, K_{O2} = 21 μM, and K_{C2} = 51 μM. Also shown is the fit (dashed line) assuming both types of binding sites have the same affinity for Ca^{2+} (K_O = 1.9 μM and K_C = 6.4 μM). Error bars represent SEM.

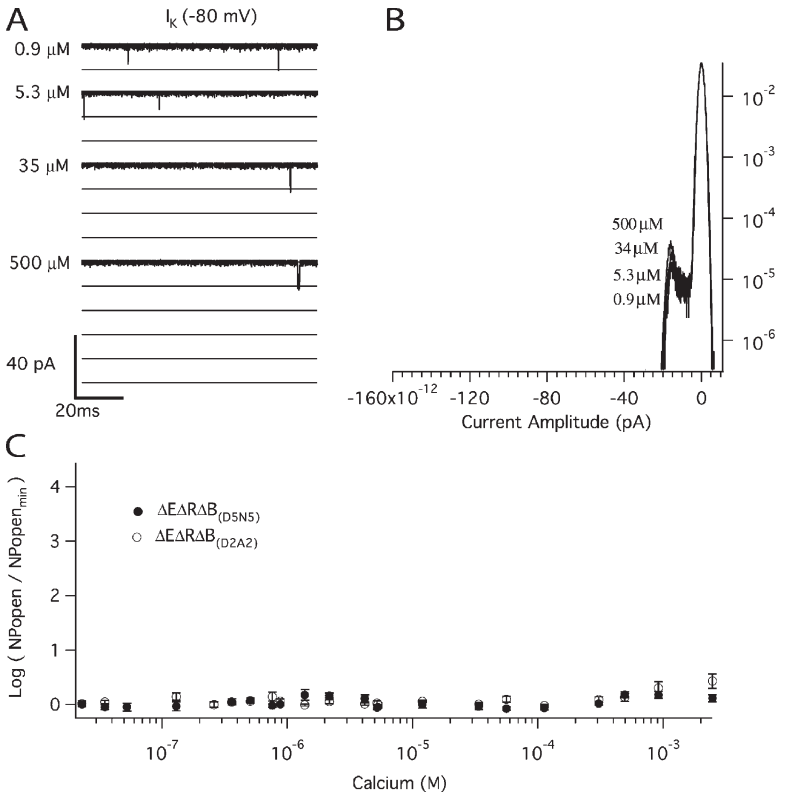

Figure 4. Mutation of all three types of Ca^{2+} binding sites eliminates the Ca^{2+} dependence of *Popen*. (A) Inward K^+ currents recorded for mutant $\Delta E\Delta R\Delta B_{(D5N5)}$ at −80 mV and filtered at 10 kHz from a macropatch in the indicated $[Ca^{2+}]$ demonstrate that *Popen* does not increase in a Ca^{2+}-dependent manner when voltage is constant. The corresponding all-points amplitude histograms are plotted in B on a semi-log scale and were constructed from 30-s recordings. (C) Dose–response relations for the effect of Ca^{2+} on *Popen* at negative voltage (−80 mV) obtained by plotting the mean log ratio of N*Popen* in the presence and absence of Ca^{2+}. For both mutant $\Delta E\Delta R\Delta B_{(D5N5)}$ (filled circles) and mutant $\Delta E\Delta R\Delta B_{(D2A2)}$, log (N*Popen*/N$Popen_{min}$) spans the entire $[Ca^{2+}]$ range but cannot be fitted because *Popen* does not vary with $[Ca^{2+}]$. Each point represents the average of between 6 and 8 patches at each $[Ca^{2+}]$ tested. Error bars represent SEM.

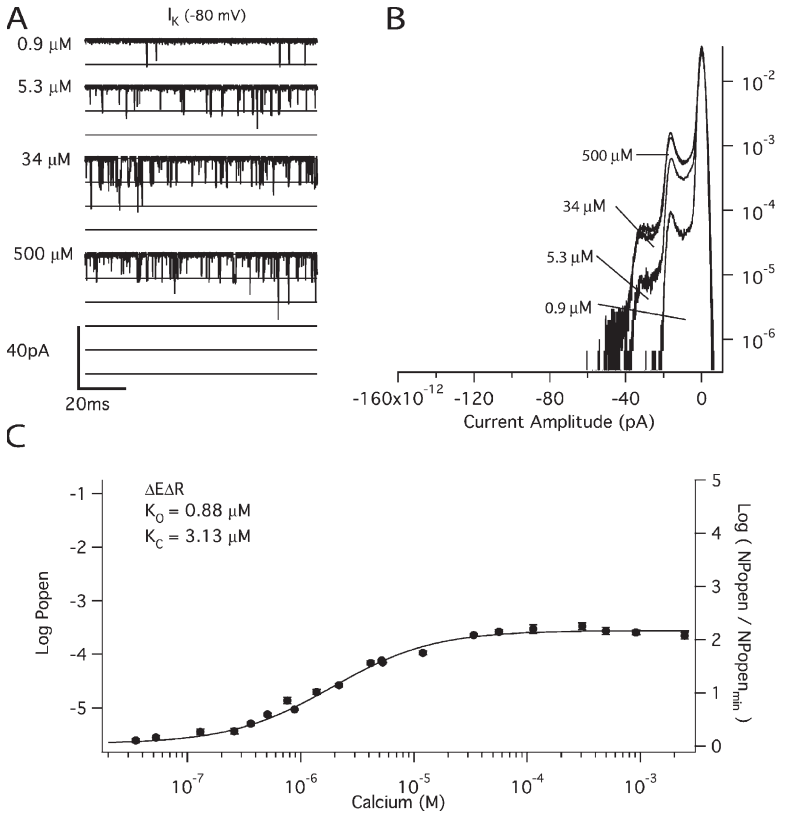

Figure 5. The Ca^{2+} binding affinities of the Ca^{2+} bowl site at −80 mV. (A) Inward K^+ currents recorded from mutant ΔEΔR at −80 mV and filtered at 10 kHz from a macropatch exposed to the indicated $[Ca^{2+}]$ demonstrate that *Popen* increases in a Ca^{2+}-dependent manner when voltage is constant. The corresponding all-point amplitude histograms are plotted in B on a semi-log scale and were constructed from 30-s recordings as in Fig. 2. The dose–response relation for the effect of $[Ca^{2+}]$ on *Popen* (left axis) and N*Popen*/N$Popen_{min}$ (right axis) at negative voltage (−80 mV) is shown in C. Each point represents the average of between 6 and 11 patches at each $[Ca^{2+}]$ tested. Log (N*Popen*/N$Popen_{min}$) spans the entire $[Ca^{2+}]$ range and is fit (solid line) by Eq. 6 yielding values of K_O = 0.88 μM and K_C = 3.13 μM. Error bars represent SEM.

the intact Ca^{2+} bowl site were then determined from a fit (solid line) with Eq. 6 below, which is analogous to Eq. 5, but represents the case where there is only one type of Ca^{2+} binding site (Horrigan and Aldrich, 2002).

$$\frac{Popen(Ca)}{Popen(0)} = \frac{(1+[Ca]/K_O)^4}{(1+[Ca]/K_C)^4} \quad (6)$$

Of importance here, Eq. 6 contains only the channel's open- and closed-state Ca^{2+} dissociation constants as free parameters, and in the limit of high [Ca^{2+}], Eq. 6 becomes:

$$\frac{Popen(Ca)}{Popen(0)} = \frac{(K_C)^4}{(K_O)^4} = C^4, \quad (7)$$

or equivalently:

$$\log\frac{Popen(Ca)}{Popen(0)} = \log\frac{K_C{}^4}{K_O{}^4} = 4\log C. \quad (8)$$

Thus, the change in log (*Popen*) from 0 to saturating [Ca^{2+}], which is the distance along the vertical axis spanned by the data in Fig. 5 C, depends only on the ratio of the open and closed conformation Ca^{2+} dissociation constants. This means that measuring *Popen* precisely at both the top and the bottom of the curve—as we have done here with unitary current recordings—places an important constraint on the fitting. Indeed, because the amplitude of the curve is determined by *C*, this leaves only one parameter free to determine the shape of the curve, either K_C or K_O. Thus, in fitting with Eq. 6, the fit is highly constrained, and it is therefore remarkable how well Eq. 6 fits the data (solid line). The fit yields the following Ca^{2+} dissociation constants for the Ca^{2+} bowl (K_O = 0.88 ± 0.06 μM; K_C = 3.13 ± 0.22 μM; C = 3.55) (see also Table I), and it is of note that they are similar to the K_{CI} and K_{OI} values estimated from the ΔE data in Fig. 3.

Ca^{2+} Binding at the RCK1 Site

Similarly, to determine the affinities of the RCK1 site, we examined the effect of Ca^{2+} on the open probability of the mutant (E399N) (D898A/D900A), which we refer to as $\Delta E\Delta B_{(D2A2)}$. The two D→A mutations render the Ca^{2+} bowl nonfunctional (Bao et al., 2004). Fig. 6 A shows unitary $\Delta E\Delta B_{(D2A2)}$ currents recorded at −80 mV with various [Ca^{2+}] from a patch that contained hundreds of channels. Corresponding amplitude histograms are shown in Fig. 6 B, and the Ca^{2+} dose–response relation we acquired for the $\Delta E\Delta B_{(D2A2)}$ channel at −80 mV is shown in Fig. 6 C (open squares). In fact, both $\Delta E\Delta B_{(D2A2)}$ and another Ca^{2+} bowl mutation, (D897N/D898N/D899N/D900N/D901N) ($\Delta E\Delta B_{(D5N5)}$), were analyzed (Fig. 6 C, closed squares), and both mutations behave similarly. The affinity of the RCK1 site was then estimated by fitting Eq. 6 to the two datasets in Fig. 6 C. The fits yielded similar values (K_O = 4.9 ± 0.6 μM; K_C = 23.2 ± 2.6 μM; C = 4.75) for $\Delta E\Delta B_{(D2A2)}$ and (K_O = 5.6 ± 0.8 μM; K_C = 26.8 ± 3.8 μM; C = 4.75) for $\Delta E\Delta B_{(D5N5)}$ (see Table I). Thus, the RCK1 site binds Ca^{2+} more weakly than does the Ca^{2+} bowl site, both when the channel is open and when it is closed (Ca^{2+} bowl: K_O = 0.88 ± 0.06 μM; K_C = 3.13 ± 0.22 μM; C = 3.55 from Fig. 5), but it has a 36% larger C value and thus a bigger effect on opening at saturating [Ca^{2+}]. This is illustrated graphically in Fig. 7, where the $\Delta E\Delta R$ (closed triangles) and $\Delta E\Delta B_{(D2A2)}$ (closed squares) Ca^{2+} dose–response curves are overlaid.

With regard to Figs. 5 and 6, however, it is interesting to note that Eq. 6 fits the data from the $\Delta E\Delta R$ channel (Fig. 5) better than it does those from the $\Delta E\Delta B_{(D5N5)}$ and $\Delta E\Delta B_{(D2A2)}$ channels (Fig. 6 C). That is, the idea represented by Eq. 6 does not appear to be as good an approximation of reality for the RCK1 site as it does the Ca^{2+} bowl site. To try to improve the fit, we have added a cooperativity factor by which the binding at one site influences binding at sites on adjacent subunits. If we call this factor *f*, and suppose for simplicity that *f* is the same for the opened and closed channel, then Eq. 9 below represents this idea (Cox et al., 1997, scheme III and discussion page 269).

$$\frac{Popen(Ca)}{Popen(0)} \approx \quad (9)$$
$$\frac{(1+4K_O[Ca]+(4K_O{}^2f+2K_O{}^2)[Ca]^2+4K_O{}^3f^2[Ca]^3+K_O{}^4f^4[Ca]^4)}{(1+4K_C[Ca]+(4K_C{}^2f+2K_C{}^2)[Ca]^2+4K_C{}^3f^2[Ca]^3+K_C{}^4f^4[Ca]^4))}$$

TABLE I

BK_{Ca} Channel Ca^{2+} Binding Parameters

Binding Site	Membrane Potential (*mV*)	K_C (*μM*)	K_O (*μM*)	*M*	*f*	*C*
Ca^{2+} Bowl						
$\Delta E\Delta R$	−80	3.1 ± 0.2	0.88 ± 0.06			3.55
$\Delta E\Delta R$	0	3.1	0.88			3.55
RCK1						
$\Delta E\Delta B_{(D2A2)}$	−80	23.2 ± 2.6	4.9 ± 0.6			4.75
$\Delta E\Delta B_{(D5N5)}$	−80	26.8 ± 3.8	5.6 ± 0.8			4.75
$\Delta E\Delta B_{(D2A2)}$ + Cooperativity	−80	13.7 ± 2.3	2.8 ± 0.5		0.45 ± 0.1	
$\Delta E\Delta B_{(D5N5)}$+ Cooperativity	−80	9.4 ± 1.8	1.8 ± 0.2		0.27 ± 0.05	
$\Delta E\Delta B_{(D2A2)}$	0	15.8 ± 3.1	2.10 ± 0.4	1.8×10^7		7.52

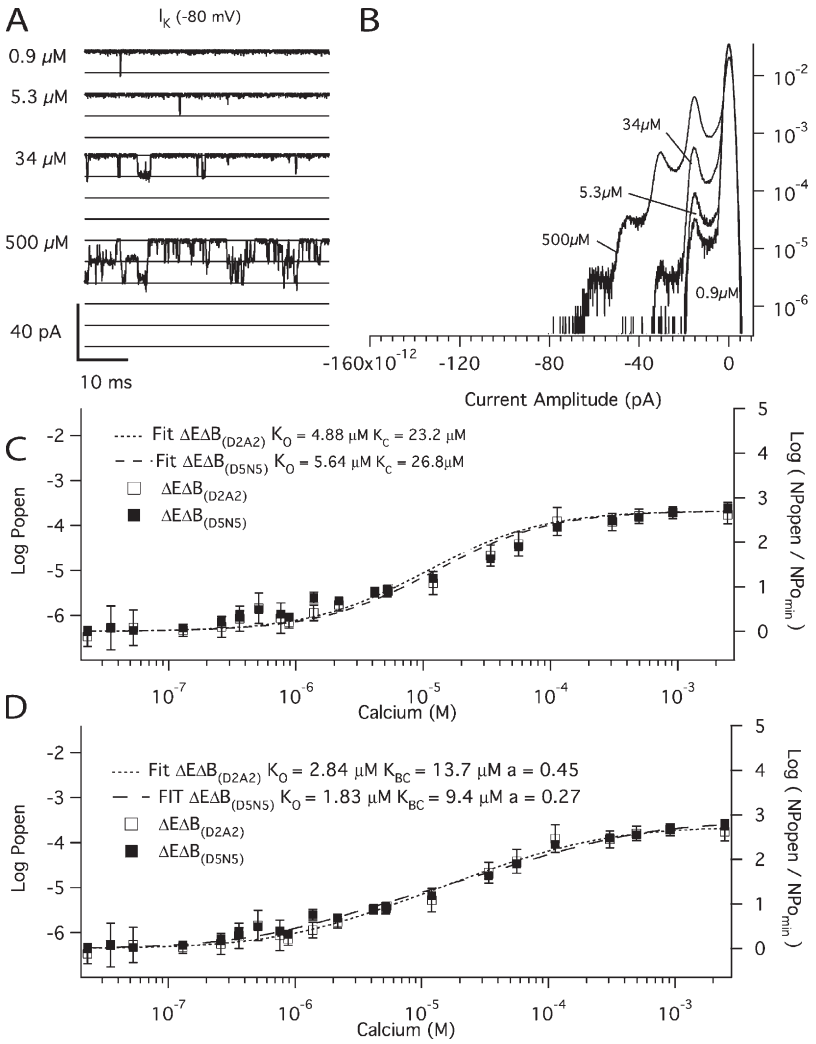

Figure 6. The Ca^{2+} binding affinities of the high-affinity RCK1 site at −80 mV. (A) Inward K^+ currents recorded from mutant $\Delta E\Delta B_{(D2A2)}$ at −80 mV and filtered at 10 kHz from a macropatch in the indicated [Ca^{2+}] demonstrate that *Popen* increases in a Ca^{2+}-dependent manner when voltage is constant. The corresponding all-points amplitude histograms are plotted in B on a semi-log scale and were constructed from 30-s recordings. The dose–response relation for the effect of Ca^{2+} on *Popen* (left axis) and N*Popen*/N$Popen_{min}$ (right axis) at negative voltage (−80 mV) is shown in C. Each point represents the average of between 6 and 16 patches at each Ca^{2+} concentration tested. For mutant $\Delta E\Delta B_{(D2A2)}$ (open squares), log (N*Popen*/N$Popen_{min}$) spans the entire [Ca^{2+}] range and is fitted (dotted line) by Eq. 6 yielding values of K_O = 4.9 μM of K_C = 23.2 μM. For mutant $\Delta E\Delta B_{(D5N5)}$ (closed squares), the fit (dashed line) yields values of K_{OB} = 5.6 μM and K_{CB} = 26.8 μM. (D) The data were also fitted with Eq. 7, which incorporates an interaction between binding sites. For mutant $\Delta E\Delta B_{(D2A2)}$ (open squares), the fit yielded values of K_O = 2.8 μM, K_C = 13.7 μM, and f = 0.45. For mutant $\Delta E\Delta B_{(D5N5)}$ (closed squares), the fit (dashed line) yielded K_O = 1.8 μM, K_C = 9.4 μM, and f = 0.27. Error bars represent SEM.

Fitting the $\Delta E\Delta B_{(D2A2)}$ data in Fig. 6 with Eq. 9 did produce better fits (Fig. 6 D) and yielded $f = 0.45 \pm 0.1$, K_C = 13.7 ± 2.3 μM, and K_O = 2.8 ± 0.5 μM for the $\Delta E\Delta B_{(D2A2)}$ channel and $f = 0.27 \pm 0.05$, K_C = 9.4 ± 1.8 μM, and K_O = 1.8 ± 0.2 μM for the $\Delta E\Delta B_{(D5N5)}$ channel (see Table I). The fact that f is <1 for both fits suggests that, if this explanation is correct, Ca^{2+} binding at one RCK1 site negatively influences Ca^{2+} binding at other RCK1 sites on adjacent subunits.

To improve the fit to the ΔEΔB data we also considered a ring model. It has been proposed that the BK_{Ca} channel has a gating ring that hangs below the channel and expands upon Ca^{2+} binding, and that this expansion pulls open the channel (Jiang et al., 2002; Kim et al., 2008). If ring expansion and channel opening are strictly coupled, such that one does not occur without the other, this idea is mathematically equivalent to the simple MWC-like allosteric models we have used thus far. If, however, ring expansion favors opening, but is not obligate for opening, they are not equivalent. A model for this situation is as follows:

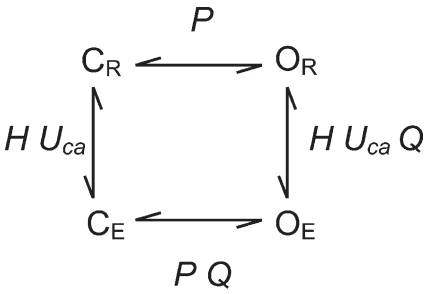

Ring Model

where P represents the equilibrium constant for channel opening when the ring is relaxed. H represents the equilibrium constant for ring expansion when the channel is closed, and no Ca^{2+} is bound. Q represents the factor by which ring expansion favors channel opening, and U_{Ca} represents the Ca^{2+}-dependent factor by which Ca^{2+} binding favors ring expansion. Then, for *Popen* we have:

$$Popen = \frac{P(1 + HU_{Ca}Q)}{1 + HU_{Ca} + P(1 + HU_{Ca}Q)}, \quad (10)$$

where

$$U_{Ca} = \frac{(1+[Ca]/K_{E1})^4(1+[Ca]/K_{E2})^4}{(1+[Ca]/K_{R1})^4(1+[Ca]/K_{R2})^4}, \quad (11)$$

or

$$U_{Ca} = \frac{(1+[Ca]/K_{E})^4}{(1+[Ca]/K_{R})^4}, \quad (12)$$

and $(Popen/Popen_{\min})$ at low open probabilities is:

$$\frac{Popen}{Popen_{\min}} \approx \frac{(1+HU_{Ca}Q)(1+H)}{(1+HU_{Ca})(1+HQ)}. \quad (13)$$

Thus, we fit the data in Fig. 6 with Eq. 13. In the fitting, however, we found that to get an acceptable fit, H had to be small (at most 0.001) and Q had to be large (at least 1,000), and when this is the case, the ring model becomes mathematically equivalent to the MWC-like model we used above, and it yields the same fits. Thus, we could not improve the fit via a ring model, and we view the fact that the best ring model fits were obtained with small values of H and large values of Q as evidence that, if the BK_{Ca} channel has a gating ring, its expansion is tightly coupled to channel opening such that one seldom occurs without the other.

The Two Sites Are Less Than Additive

Can the affinities measured for each binding site in isolation, when combined, explain the effect of Ca^{2+} when both binding sites are intact? To answer this question we calculated the predicted $Popen(Ca^{2+})/Popen(0)$ versus $[Ca^{2+}]$ curve for the ΔE channel based on the affinities measured for each high-affinity Ca^{2+} binding site in Figs. 5 C and 6 C. In Fig. 7 this prediction (dark solid curve) is compared with the ΔE data (filled circles). Of most interest, the predicted curve, although similar to the data, does not everywhere overlay the data, but rather it predicts a larger response to Ca^{2+} than is observed. We might consider two possible reasons for this outcome. The first is that one or the other of the mutations we have used is not completely selective. That is, in addition to eliminating Ca^{2+} sensing via one type of Ca^{2+} binding site, a given mutation may also affect Ca^{2+} binding at the other site. We do not favor this explanation, however, because in order for it to explain the data, the mutation would have to eliminate Ca^{2+} binding at one site while augmenting it at the other. Although this cannot be ruled out, it seems unlikely. The second potential explanation is that there is negative cooperativity between Ca^{2+} binding sites, such that their individual influences are naturally less than what is observed when they are combined. Pursuing this idea further we have calculated that a cooperativity factor between the RCK1 and Ca^{2+} bowl Ca^{2+} binding sites on the same subunit of 1, when the channel is closed (no cooperativity), and 0.75, when the channel is open (negative cooperativity), could explain this effect (Fig. 7, gray curve).

Do These Results Explain the G-V Shifts with $[Ca^{2+}]$?

Another question of interest is do the binding affinities we have measured at a single voltage (−80 mV) explain the BK_{Ca} channel's sensitivity to Ca^{2+} over a range of voltages? Fig. 8 A shows the mSlo G-V relation at a series of $[Ca^{2+}]$ fit simultaneously with the BK_{Ca}-gating model of Horrigan and Aldrich (2002) (the HA model) but modified to include two sets of Ca^{2+} binding sites, four per set. There were no free parameters in this fit, but rather gating parameters determined from these and previous experiments (Bao and Cox, 2005) were used. The parameters were as follows: K_{O1} = 0.88 μM; K_{C1} = 3.13 μM; K_{O2} = 4.88 μM; K_{C2} = 23.2 μM; L_O = 2e-06; z_L= 0.41 e; V_{hc} = 151 mV; V_{ho} = 27 mV; and Z_J = 0.58 e. The allosteric factors E_1 and E_2 were set to 1 to simulate no interaction between voltage–sensor movement and Ca^{2+} binding at either site. The fit is poor. The model responds to Ca^{2+} less than is required to move the model G-V

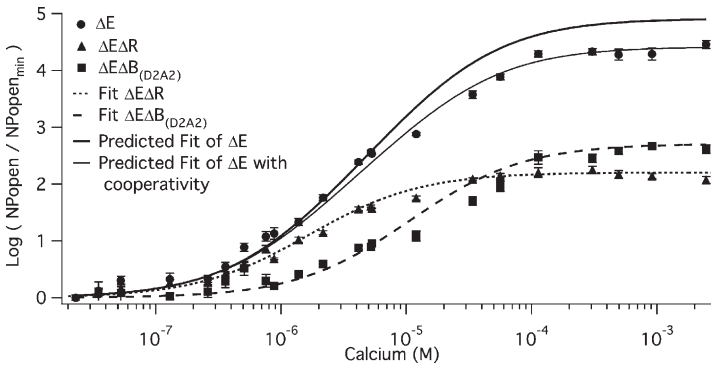

Figure 7. The two binding sites are less than additive. The mean log ratio of N*Popen* at −80 mV in the presence and absence of Ca^{2+} for mutants ΔE (solid circles), ΔEΔR (solid triangles), and $\Delta E\Delta B_{(D2A2)}$ (solid squares) are plotted versus $[Ca^{2+}]$. Various fits of log (N*Popen*/N$Popen_{\min}$) are superimposed on the data. The fit of ΔEΔR also displayed in Fig. 2 is shown as a short dashed curve. The fit of $\Delta E\Delta B_{(D2A2)}$ also displayed in Fig. 3 is shown as a long dashed curve. We simulated the log (N*Popen*/N$Popen_{\min}$) relation (dark solid line) predicted by the affinities determined from each of the mutants using Eq. 5. The parameters of the fit were: K_{O1} = 0.88 μM, K_{C1} = 3.13 μM, K_{O2} = 4.88 μM, and K_{C2} = 23.2 μM. Also plotted (gray curve) is a fit that incorporates cooperativity between the binding sites. The equation for the fit was log (N*Popen*/N$Popen_{\min}$) = $((1+(K_{O1}+K_{O2})+K_{O1}K_{O2}b)^4)$ / $((1+(K_{C1}+K_{C2})+K_{C1}K_{C2}a)^4)$. The parameters of the fit were: K_{O1} = 0.88 μM, K_{C1} = 3.13 μM, K_{O2} = 4.88 μM, K_{C2} = 23.2 μM, a = 1, and b = 0.75. Error bars represent SEM.

relation along with the data. Interestingly, however, when we let E_1 and E_2 vary freely, that is, we allowed interactions between binding sites and voltage sensors, the fit markedly improved ($E_i = 1.43$; $E_2 = 1.73$) (Fig. 8 B). This suggests that voltage-sensor movement may alter Ca^{2+} binding and vice versa.

Voltage Affects Ca^{2+} Binding

To test this hypothesis directly, we repeated the experiments so far described, but changed the voltage from −80 to 0 mV. We reasoned that at −80 mV few voltage sensors would be active (5% or less) (Stefani et al., 1997; Horrigan and Aldrich, 1999, 2002; Bao and Cox, 2005), and thus there would be very little influence of voltage-sensor movement on Ca^{2+} binding. But at 0 mV, where the channels' voltage sensors are active 35% of the time

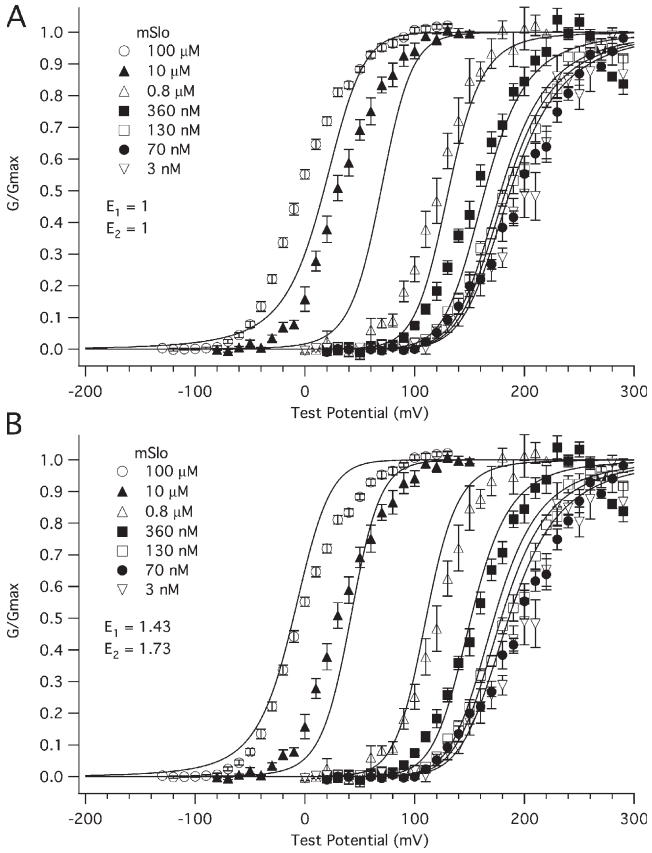

Figure 8. Voltage likely affects the affinity of the BK_{Ca} channel for Ca^{2+}. Shown are a series of mSlo1α G-V relations determined at the following [Ca^{2+}]: 0.003, 0.070, 0.130, 0.360, 0.8, 10, and 100 µM and fitted simultaneously with the HA model modified to include two Ca^{2+} binding sites (Bao et al., 2002; Horrigan and Aldrich, 2002). Using values determined from this and previous experiments in our laboratory (Bao and Cox, 2005), the parameters were held as follows: $K_{O1} = 0.88$ µM, $K_{C1} = 3.18$ µM, $K_{O2} = 4.88$ µM, $K_{C2} = 23.2$ µM, $L_O = 2.2 \times 10^{-6}$, $z_L = 0.41$ *e*, $V_{hc} = 151$ mV, $V_{ho} = 27$ mV, and $z_J = 0.58$ *e*. In A, the values of allosteric factors E_1 and E_2 were held to a value of 1 for both Ca^{2+} binding sites A and B. In B, the values of E_1 and E_2 were allowed to vary. The best fit values of E_1 and E_2 were 1.43 and 1.73, respectively.

when the channels are open (Horrigan and Aldrich, 1999, 2002; Bao and Cox, 2005), if voltage-sensor movement affects Ca^{2+} binding, some influence of the change in voltage should be observed. Shown in Fig. 9 (A and C) are the $Popen(Ca^{2+})/Popen(0)$ versus [Ca^{2+}] curves derived from these experiments (open symbols) along with their counterparts determined at −80 mV (filled symbols). Examining first the ΔEΔR channel (Fig. 9 A), we see that its 0- and −80-mV $Popen(Ca^{2+})/Popen(0)$ versus [Ca^{2+}] curves superimpose. This indicates that voltage-sensor movement does not affect Ca^{2+} binding at the Ca^{2+} bowl, but rather a change in voltage simply slides the *Popen* versus [Ca^{2+}] curve up the *Popen* axis (see Fig. 9 B). Conversely, there is a substantial effect of voltage on Ca^{2+} binding at the RCK1 sites (Fig. 9, C and D). The maximal effect of Ca^{2+} on the open probability of the $\Delta E\Delta B_{(D2A2)}$ channel is ∼10-fold larger at 0 mV than it is at −80 mV (Fig. 9 C), and fitting the 0 mV curve in Fig. 9 C with Eq. 6 yields Ca^{2+} dissociation constants of 15.6 ± 2.5 µM and 2.1 ± 0.3 µM ($C = 7.39$), as compared with 23.2 ± 2.6 µM and 4.9 ± 0.6 µM ($C = 4.75$) at −80 mV.

It is not rigorously correct, however, to fit the 0 mV $\Delta E\Delta B_{(D2A2)}$ data in Fig. 9 C with Eq. 6, as an assumption underlying this equation is that *Popen* is never greater than $\sim 10^{-2}$. Although this is the case for the ΔEΔR and ΔEΔB channels at −80 mV, as shown in Fig. 9 D, it is not the case for the $\Delta E\Delta B_{(D2A2)}$ channel at 0 mV. Thus, to determine the dissociation constants of the RCK1 sites at 0 mV, we fit the $\Delta E\Delta B_{(D2A2)}$ *Popen* versus [Ca^{2+}] curve in Fig. 9 D with Eq. 14 below, which does not require this assumption.

$$P_{open} = \frac{M(1+[Ca]/K_O)^4}{(1+[Ca]/K_C)^4 + M(1+[Ca]/K_O)^4} \qquad (14)$$

This yielded (Fig. 9 D, solid curve) $K_C = 15.8 \pm 3.1$ µM, $K_O = 2.10 \pm 0.4$ µM ($C = 7.52$), and $M = 1.8 \times 10^{-5} \pm 0.5 \times 10^{-5}$ (see Table I). Thus, changing the voltage from −80 mV to 0 mV decreases K_C at the RCK1 Ca^{2+} binding site by a factor of 0.7 (23.2→15.8). It decreases K_O by a factor of 0.4 (4.88→2.10), and it increases C by a factor of 1.8. This increase in C makes the efficacy of the RCK1 sites an order of magnitude larger than the efficacy of the Ca^{2+} bowl sites at 0 mV. This is highlighted in Fig. 10, where the 0 mV Ca^{2+} dose-response curves for the two sites are superimposed. Also evident, at 0 mV, as we saw at −80 mV, the ΔE channel's Ca^{2+} dose-response curve spans a smaller range of open probabilities than is predicted (Fig. 10, dark solid curve) by the combination of the fits to each individual dose-response curve. And again, we can explain this effect by supposing negative cooperativity between the RCK1 and the Ca^{2+} bowl sites in each subunit. A cooperativity factor of 1 when the channel is closed (no cooperativity) and 0.65 when the channel is open (negative cooperativity) produced the best fit (Fig. 10, gray curve).

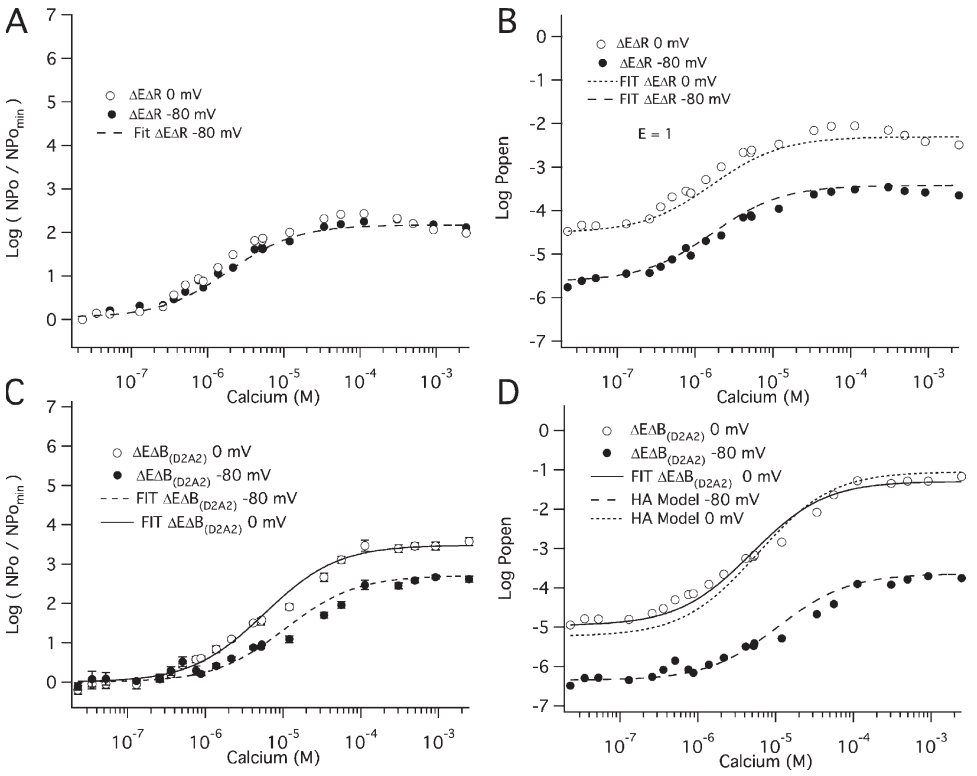

Figure 9. The Ca^{2+} dependence of *Popen* for the RCK1 site is affected by voltage. However, voltage does not alter the binding at the Ca^{2+} bowl site. (A) The mean log ratio of N*Popen/NPopen*$_{min}$ versus [Ca^{2+}] for mutant ΔEΔR is shown for patches held at 0 mV (open circles) or at −80 mV (solid circles). Each point represents the average of between 6 and 13 patches at each Ca^{2+} concentration tested. Shown is the fit (dashed curve) of N*Popen/*N*Popen*$_{min}$ based on Eq. 6 and previously shown in Fig. 5. The values determined from the fit are: K_O = 0.88 μM and K_C = 3.13 μM. (B) The mean log *Popen* versus [Ca^{2+}] relation for mutant ΔEΔR at both 0 and −80 mV are well fitted with the HA model using the Ca^{2+} binding constants determined. The values for the parameters were held as follows: K_O = 0.88 μM, K_C = 3.18 μM, $L_O = 6.3 \times 10^{-6}$, $z_L = 0.41$ *e*, $V_{hc} = 151$ mV, V_{ho} = 27 mV, z_J = 0.58 *e*, and E = 1. (C) The N*Popen/NPopen*$_{min}$ versus [Ca^{2+}] relation for mutant $\Delta E\Delta B_{(D2A2)}$ is shown for patches held at 0 mV (open circles) or at −80 mV (solid circles). Each point represents the average of between 6 and 14 patches at each [Ca^{2+}] tested. The N*Popen/*N*Popen*$_{min}$ versus Ca^{2+} relations are fitted with Eq. 6. The values of the fit parameters are: $\Delta E\Delta B_{(D2A2)}$: −80 mV, K_O = 4.9 μM and K_C = 23.2 μM; $\Delta E\Delta B_{(D2A2)}$: 0 mV, K_O = 2.1 μM and K_C = 15.6 μM. (D) The mean log *Popen* versus [Ca^{2+}] relation for mutant $\Delta E\Delta B_{(D2A2)}$ at both 0 and −80 mV. First, the 0 mV data were fitted by Eq. 14 to yield the values: K_O = 2.1 μM and K_C = 15.8 μM. The data were also fitted with the HA model. The parameters were held as follows: K_O = 4.9 μM, K_C = 23.2 μM, $L_O = 1.2 \times 10^{-6}$, z_L = 0.41 *e*, V_{hc} = 151 mV, V_{ho} = 27 mV, z_J = 0.58 *e*, and E = 6.03.

We could explain the effect of voltage on Ca^{2+} binding at the RCK1 sites in terms of the HA model by supposing that as the channel's voltage sensors move to their active conformation, they alter the affinity of the channel's RCK1 sites by a factor *E* (Horrigan and Aldrich, 2002). To estimate *E*, we fit the *Popen* versus [Ca^{2+}] curves at both −80 and 0 mV in Fig. 9 D simultaneously with the HA model. We held the voltage sensing parameters: V_{hc} V_{ho} z_J and z_L to values previously determined for the mSlo channel (Bao and Cox, 2005).

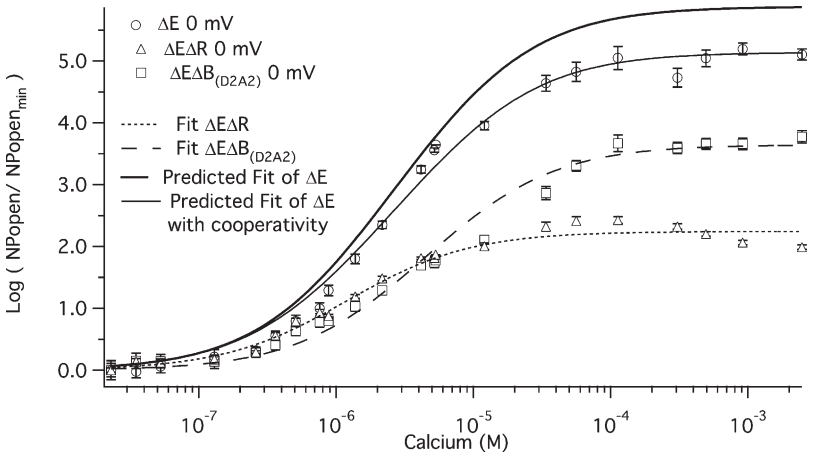

Figure 10. The two binding sites are less than additive at 0 mV. The mean log ratio of N*Popen* at 0 mV in the presence and absence of Ca^{2+} for mutants ΔE (open circles), ΔEΔR (open triangles), and $\Delta E\Delta B_{(D2A2)}$ (open squares) are plotted versus [Ca^{2+}]. Each point represents the average of between 6 and 14 patches at each [Ca^{2+}] tested. Various fits of log (N*Popen/*N*Popen*$_{min}$) are superimposed on the data. The fit of ΔEΔR (short dashed line) with Eq. 6 yielded values of K_O = 0.63 μM and K_C = 2.28 μM. The fit of $\Delta E\Delta B_{(D2A2)}$ (long dashed curve) yielded values of K_O = 1.56 μM and K_C = 12.7 μM. Using the same equation, we simulated the log (N*Popen/*N*Popen*$_{min}$) versus Ca^{2+} relation (dark solid line) predicted by the affinities determined for each site in isolation. The parameters of the fit were: K_{O1} = 0.63 μM, K_{C1} = 2.28 μM, K_{O2} = 1.56 μM, and K_{C2} = 12.7 μM. Also plotted (gray curve) is a log (N*Popen/*N*Popen*$_{min}$) versus [Ca^{2+}] fit that incorporates cooperativity between binding sites. The equation for the fit was log (N*Popen/*N*Popen*$_{min}$) = $((1+(K_{O1}+K_{O2})+K_{O1}K_{O2}b)^4) / ((1+(K_{C1}+K_{C2})+K_{C1}K_{C2}a)^4)$. The parameters of the fit were: K_{O1} = 0.63 μM, K_{C1} = 2.28 μM, K_{O2} = 1.56 μM, K_{C2} = 12.7, a = 1, and b = 0.65. Error bars represent SEM.

We held K_C and K_O to the values we determined in this study at −80 mV. We set *L(0)* to the value determined by the bottom of the *Popen* versus [Ca^{2+}] curve at −80 mV, and we allowed only *E* to vary. Remarkably, both RCK1 site Ca^{2+} dose-response curves, −80 and 0 mV, could be fitted fairly well with the same parameters with *E* equal to 6.03 (Fig. 9 D, dotted line).

The value of *E* estimated in this way, however, is dependent on the voltage-sensing parameters of the model (V_{ho} V_{hc}, z_L and z_J), parameters that we have taken from previous experiments with wild-type mSlo channels. As here, however, we are using the mutant E399N as our background channel. It may be that this mutation alters one or more of these parameters and thereby renders this method inaccurate. Indeed, differences between the mSlo and E399N G-V curves in the absence of Ca^{2+} (unpublished data) make us think this may be the case. Thus, another approach we have taken to determining *E* for the wild-type mSlo channel's RCK1 site is to fit the wild-type channel's G-V relation as a function of [Ca^{2+}] with a two-Ca^{2+} binding site HA model that includes a voltage sensor–Ca^{2+} binding site interaction factor *E* for only one of the high-affinity binding sites, the one with lower affinities. That is:

$$P_{open} = \frac{T_O}{T_C + T_O}$$

where (15)

$$T_C = \left(1 + K_{C1} + K_{C2} + K_{C1}K_{C2} + J_C\left(1 + K_{C1} + K_{C2}E + K_{C1}K_{C2}E\right)\right)^4$$

$$T_O = \left(1 + K_{O1} + K_{O2} + K_{O1}K_{O2} + J_O\left(1 + K_{O1} + K_{O2}E + K_{O1}K_{O2}E\right)\right)^4$$

where

$$L = L(0)e^{\frac{z_g FV}{RT}};$$

$$J_O = e^{\frac{z_J F(V - V_{ho})}{RT}};$$

$$J_C = e^{\frac{z_J F(V - V_{hc})}{RT}};$$

$$K_{C1} = \frac{[Ca]}{K_{C1}},$$

$$K_{C2} = \frac{[Ca]}{K_{C2}};$$

$$K_{O1} = \frac{[Ca]}{K_{O1}},$$

$$K_{O2} = \frac{[Ca]}{K_{O2}}.$$

We held all parameters but *E* to values that have been independently determined either here or previously (Bao and Cox, 2005) and allowed only *E* to vary. The resulting best fit from this approach is shown in Fig. 11. It shows that even with these severe constraints, the two-site HA model with our newly determined Ca^{2+} binding constants can approximate the shifting of the mSlo channel's G-V relation as a function of [Ca^{2+}], and remarkably the fit yields *E* = 2.8, a value that is very similar to the value of *E* (2.4) estimated independently by Horrigan and Aldrich (2002) from measurements of the

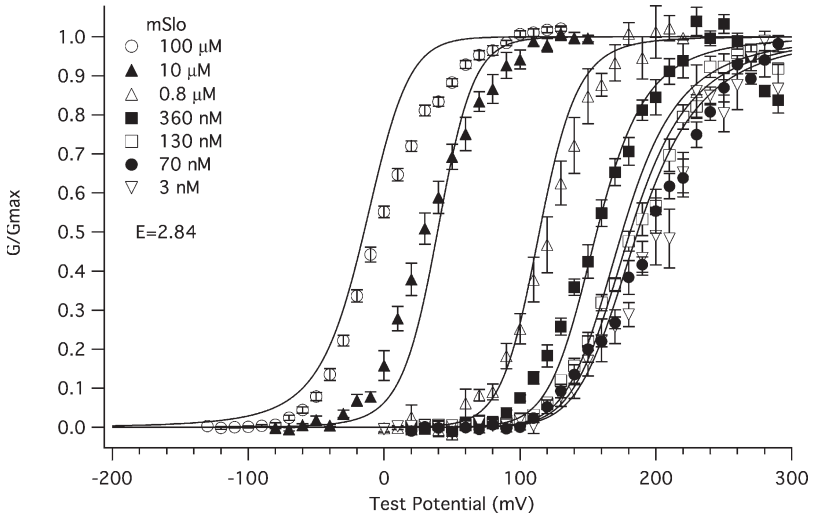

Figure 11. A modified HA model can explain the effect of Ca^{2+} on the steady-state gating properties of the BK_{Ca} channel. Shown are series of mSlo1α G-V relations determined at the following [Ca^{2+}]: 0.003, 0.070, 0.130, 0.360, 0.8, 10, and 100 µM and fit simultaneously with the modified model that includes two types of Ca^{2+} binding sites, one type interacts with the voltage sensor, and the other type is independent. The data are the same as shown in Fig. 8. The parameters were held as follows: K_{O1} = 0.88 µM, K_{C1} = 3.18 µM, K_{O2} = 4.88 µM, K_{C2} = 23.2 µM, $L_O = 2.2 \times 10^{-6}$, z_L = 0.41 *e*, V_{hc} = 151 mV, V_{ho} = 27 mV, and z_J = 0.58 *e*. The value of E coupling voltage sensor activation and Ca^{2+} binding at one type of site was allowed to vary. Shown is the best fit obtained. The value of E was calculated to be 2.84 ± 0.13.

channel's gating charge movement as a function of voltage at 0 and 70 μM [Ca^{2+}]. Thus, we currently favor this estimate.

DISCUSSION

Here, we have measured the Ca^{2+} binding constants of the BK_{Ca} channel's two types of high-affinity Ca^{2+} binding sites. To be as accurate as possible, we used unitary current recordings from patches containing from a few hundred to just a few channels. This allowed us to determine *Popen* over five orders of magnitude. To be as model-independent as possible, as pioneered by Horrigan and Aldrich (2002), we have made measurements at constant voltage and low *Popen*, such that the amplitudes and shapes of the resulting Ca^{2+} dose-response curves were dependent only on the channel's Ca^{2+} binding parameters. Further, to prevent potential interactions between Ca^{2+} binding sites and voltage sensors from complicating our analysis, our initial experiments were done at −80 mV, where the BK_{Ca} channel's voltage sensors are very seldom active. The essential assumptions we made in fitting our data were as follows: (1) that there is a single conformational change between open and closed that can occur with any number of Ca^{2+} bound (this idea is consistent with a great many single-channel and macroscopic BK_{Ca} channel studies and all current models) (McManus and Magleby, 1991; Cox et al., 1997; Cui et al., 1997; Horrigan and Aldrich, 1999, 2002; Horrigan et al., 1999; Rothberg and Magleby, 1999, 2000; Cox and Aldrich, 2000); and (2) that there are four of each type of high-affinity site. This has been established for the Ca^{2+} bowl (Niu and Magleby, 2002), and given the fourfold symmetry of the channel, it seems likely to be the case for the RCK1 site as well.

Of primary interest, we found that the Ca^{2+} bowl's dose-response curve at −80 mV could be well fitted by supposing that each Ca^{2+} bowl independently influences opening, and that each site has an affinity of 3.13 ± 0.22 μM when the channel is closed and 0.88 ± 0.06 μM when the channel is open. These values produce a C value of 3.55, which allows us to calculate that each bound Ca^{2+} at a Ca^{2+} bowl decreases the energy difference between open and closed by 3.1 KJ/mol. These numbers may be compared with previous estimates of K_C and K_O for this site. Xia et al. (2002) estimated K_C = 4.5 ± 1.7 μM and K_O = 2.0 ± 0.7 (C = 2.25), and Bao et al. (2002) estimated K_C = 3.8 ± 0.2 and K_O = 0.94 ± 0.06 (C = 4.0). Thus, our current estimates are quite close to those of Bao et al. (2002) and similar as well to those of Xia et al. (2002), although their larger value of K_O (2.0 μM) reduces C to 2.2, too low to be compatible with our data. Further, we found no change in the binding properties of this site when the membrane voltage was changed from −80 to 0 mV.

At the RCK1 site we found the $\Delta E \Delta B_{(D2A2)}$ dose-response curve at −80 mV could be fitted with a K_C of 23.2 ± 2.6 μM and a K_O of 4.9 ± 0.55 μM (C = 4.75), which yields a change in the energy difference between open and closed per bound Ca^{2+} of −3.8 KJ/mol. However, in this case the fit was improved by supposing some negative cooperativity between sites. The best fit was achieved with a cooperativity factor of 0.45 ± 0.1, now with K_C = 13.7 ± 2.3 μM and K_O = 2.8 ± 0.5 μM. With either method of fitting, however, the RCK1 site has a substantially lower affinity for Ca^{2+} than does the Ca^{2+} bowl in both the closed and in the open conformation. These numbers may be compared with the previous estimates of Xia et al. (2002), K_C = 17.2 ± 4.0 μM and K_O = 4.6 ± 1.0 μM, C = 3.74, which are similar to what we have found, and those of Bao et al. (2002), K_O = 3.8 ± 0.2 μM and K_C = 0.94 ± 0.06 μM, C = 4.0, which are higher affinity than what we have found (but see next paragraph). Interestingly, and of relevance here, we have found that Ca^{2+} binding at the RCK1 site is voltage dependent. The Ca^{2+} binding affinities in both the closed and open conformation increased as the voltage was depolarized. Moving the membrane voltage from −80 to 0 mV decreased K_C from 23.2 ± 2.6 μM to 15.8 ± 3.1 μM and K_O from 4.9 ± 0.6 μM to 2.1 ± 0.4 μM. This increased C from 4.75 to 7.52. Thus, as the voltage is depolarized, Ca^{2+} ions bind more tightly to the RCK1 site in both the closed and open conformations of the channel, and the factor by which each binding event increases the equilibrium constant for opening increases ∼1.5-fold.

In light of this result, one might suppose that the binding properties of the BK_{Ca} channel's two types of high-affinity Ca^{2+} binding sites will come closer together as the membrane voltage is further depolarized and the RCK1 sites' Ca^{2+} dissociation constants become progressively smaller. Although we have not done experiments at membrane voltages more positive than 0 mV and therefore cannot here confirm this hypothesis, such an idea could explain why Qian et al. (2006), in experiments with hybrid channels containing differing numbers of functional RCK1 or Ca^{2+} bowl sites, found that channels with either just four Ca^{2+} bowl sites or just four RCK1 sites showed almost identical Ca^{2+} dose-response curves at +50 mV. Further, it may also account, at least in part, for the estimates of Bao et al. (2002) being higher affinity than what we have found here for the RCK1 site, as Bao et al.'s estimates were based on the behavior of the mutant channel's full G-V relation as a function of Ca^{2+}, and therefore they necessarily took into account *Popen* measurements at high voltage.

We have also observed that the effects of Ca^{2+} binding at each site, when measured individually, sum to more than what is observed when both sites are intact. We are unsure of the cause of this lack of strict independence, but we can explain it by supposing negative cooperativity between the Ca^{2+} bowl and RCK1 sites within the

same subunit. In fact, all that is required is weak negative cooperativity between sites when the channel is open (b = 0.75 [−80 mV] or b = 0.65 [0 mV]) and no cooperative interaction between sites when the channel is closed. Thus, perhaps as the BK_{Ca} channel opens, a negative interaction between binding sites develops. In contrast to this result, however, in a study of single hybrid BK_{Ca} channels that contained two RCK1 sites and two Ca^{2+} bowl sites either on the same or on different subunits, Qian et al. (2006) found that there was positive rather than negative cooperativity between binding sites in the same subunit. The reason for these differing conclusions is not clear to us; however, as their study was done at +50 mV and ours at lower voltages, this difference may be the most relevant factor. What we can say, however, is that the Ca^{2+} binding constants reported by Qian et al. (2006) at +50 mV are not compatible at either site with our Ca^{2+} dose-response curves recorded at −80 and 0 mV.

Finally, one might ask what is the physical mechanism by which a change in voltage influences Ca^{2+} binding at the RCK1 sites? And why does this not occur at the Ca^{2+} bowl sites. We do not yet know the answers to these questions, but our current hypothesis is that the RCK1 sites lie in close proximity to the channel's voltage-sensing domains, and that as a given voltage sensor moves, it alters the structure of its nearby RCK1 Ca^{2+} binding site, while having no such interaction at the Ca^{2+} bowl. An allosteric interaction between the BK_{Ca} channel's low-affinity Ca^{2+} binding sites (those disabled by the E399N mutation) and its voltage sensors has already been firmly established (Hu et al., 2001; Cui et al., 1997, Yang and Sachs, 1989; Cui et al., 1997; Horrigan and Ma, 2008), and like the high-affinity RCK1 sites we have investigated here, these low-affinity sites are also thought to reside in the channel's RCK1 domains. Alternatively, one might suppose that Ca^{2+} binding is voltage dependent because Ca^{2+} binds within the electric field of the membrane; however, the RCK1 domains of the channel are thought to be suspended below the channel and thus they are not likely within the membrane's electric field.

This work was supported by grant P01-HL077378 from the National Institutes of Health.

Edward N. Pugh served as editor.

Submitted: 30 July 2008
Accepted: 9 October 2008

REFERENCES

Bao, L., and D.H. Cox. 2005. Gating and ionic currents reveal how the BK_{Ca} channel's Ca2+ sensitivity is enhanced by its beta1 subunit. *J. Gen. Physiol.* 126:393–412.

Bao, L., A.M. Rapin, E.C. Holmstrand, and D.H. Cox. 2002. Elimination of the BK(Ca) channel's high-affinity Ca(2+) sensitivity. *J. Gen. Physiol.* 120:173–189.

Bao, L., C. Kaldany, E.C. Holmstrand, and D.H. Cox. 2004. Mapping the BK_{Ca} channel's "Ca2+ bowl": side-chains essential for Ca2+ sensing. *J. Gen. Physiol.* 123:475–489.

Barrett, J.N., K.L. Magleby, and B.S. Pallotta. 1982. Properties of single calcium-activated potassium channels in cultured rat muscle. *J. Physiol.* 331:211–230.

Bian, S., I. Favre, and E. Moczydlowski. 2001. Ca2+-binding activity of a COOH-terminal fragment of the Drosophila BK channel involved in Ca2+-dependent activation. *Proc. Natl. Acad. Sci. USA.* 98:4776–4781.

Brenner, R., G.J. Perez, A.D. Bonev, D.M. Eckman, J.C. Kosek, S.W. Wiler, A.J. Patterson, M.T. Nelson, and R.W. Aldrich. 2000. Vasoregulation by the beta1 subunit of the calcium-activated potassium channel. *Nature.* 407:870–876.

Butler, A., S. Tsunoda, D.P. McCobb, A. Wei, and L. Salkoff. 1993. mSlo, a complex mouse gene encoding "maxi" calcium-activated potassium channels. *Science.* 261:221–224.

Cox, D.H., and R.W. Aldrich. 2000. Role of the beta1 subunit in large-conductance Ca(2+)-activated K(+) channel gating energetics. Mechanisms of enhanced Ca(2+) sensitivity. *J. Gen. Physiol.* 116:411–432.

Cox, D.H., J. Cui, and R.W. Aldrich. 1997. Allosteric gating of a large conductance Ca-activated K+ channel. *J. Gen. Physiol.* 110:257–281.

Cui, J., D.H. Cox, and R.W. Aldrich. 1997. Intrinsic voltage dependence and Ca^{2+} regulation of *mslo* large conductance Ca-activated K^+ channels. *J. Gen. Physiol.* 109:647–673.

Diaz, L., P. Meera, J. Amigo, E. Stefani, O. Alvarez, L. Toro, and R. Latorre. 1998. Role of the S4 segment in a voltage-dependent calcium-sensitive potassium (hSlo) channel. *J. Biol. Chem.* 273: 32430–32436.

Hamill, O.P., A. Marty, E. Neher, B. Sakmann, and F.J. Sigworth. 1981. Improved patch-clamp techniques for high-resolution current recording from cells and cell-free membrane patches. *Pflugers Arch.* 391:85–100.

Horrigan, F.T., and R.W. Aldrich. 1999. Allosteric voltage gating of potassium channels II. Mslo channel gating charge movement in the absence of Ca(2+). *J. Gen. Physiol.* 114:305–336.

Horrigan, F.T., and R.W. Aldrich. 2002. Coupling between voltage sensor activation, Ca2+ binding and channel opening in large conductance (BK) potassium channels. *J. Gen. Physiol.* 120:267–305.

Horrigan, F.T., and Z. Ma. 2008. Mg2+ enhances voltage sensor/gate coupling in BK channels. *J. Gen. Physiol.* 131:13–32.

Horrigan, F.T., J. Cui, and R.W. Aldrich. 1999. Allosteric voltage gating of potassium channels I. Mslo ionic currents in the absence of Ca(2+). *J. Gen. Physiol.* 114:277–304.

Hu, H., L.R. Shao, S. Chavoshy, N. Gu, M. Trieb, R. Behrens, P. Laake, O. Pongs, H.G. Knaus, O.P. Ottersen, and J.F. Storm. 2001. Presynaptic Ca2+-activated K+ channels in glutamatergic hippocampal terminals and their role in spike repolarization and regulation of transmitter release. *J. Neurosci.* 21:9585–9597.

Jiang, Y., A. Pico, M. Cadene, B.T. Chait, and R. MacKinnon. 2001. Structure of the RCK domain from the E. coli K+ channel and demonstration of its presence in the human BK channel. *Neuron.* 29:593–601.

Jiang, Y., A. Lee, J. Chen, M. Cadene, B.T. Chait, and R. MacKinnon. 2002. Crystal structure and mechanism of a calcium-gated potassium channel. *Nature.* 417:515–522.

Kim, H.J., H.H. Lim, S.H. Rho, L. Bao, J.H. Lee, D.H. Cox, H. Kim, and C.S. Park. 2008. Modulation of the conductance-voltage relationship of the BK Ca channel by mutations at the putative flexible interface between two RCK domains. *Biophys. J.* 94:446–456.

Magleby, K.L. 2003. Gating mechanism of BK (Slo1) channels: so near, yet so far. *J. Gen. Physiol.* 121:81–96.

McManus, O.B., and K.L. Magleby. 1991. Accounting for the Ca(2+)-dependent kinetics of single large- conductance Ca(2+)-activated K+ channels in rat skeletal muscle. *J. Physiol.* 443:739–777.

Nelson, M.T., and J.M. Quayle. 1995. Physiological roles and properties of potassium channels in arterial smooth muscle. *Am. J. Physiol.* 268:C799–C822.

Niu, X., and K.L. Magleby. 2002. Stepwise contribution of each subunit to the cooperative activation of BK channels by Ca2+. *Proc. Natl. Acad. Sci. USA.* 99:11441–11446.

Qian, X., and K.L. Magleby. 2003. Beta1 subunits facilitate gating of BK channels by acting through the Ca2+, but not the Mg2+, activating mechanisms. *Proc. Natl. Acad. Sci. USA.* 100:10061–10066.

Qian, X., X. Niu, and K.L. Magleby. 2006. Intra- and intersubunit cooperativity in activation of BK channels by Ca2+. *J. Gen. Physiol.* 128:389–404.

Roberts, W.M., R.A. Jacobs, and A.J. Hudspeth. 1990. Colocalization of ion channels involved in frequency selectivity and synaptic transmission at presynaptic active zones of hair cells. *J. Neurosci.* 10:3664–3684.

Robitaille, R.E., M. Adler, and M.P. Charlton. 1993. Calcium channels and calcium-gated potassium channels at the frog neuromuscular junction. *J. Physiol. (Paris).* 87:15–24.

Rothberg, B.S., and K.L. Magleby. 1999. Gating kinetics of single large-conductance Ca2+-activated K+ channels in high Ca2+ suggest a two-tiered allosteric gating mechanism. *J. Gen. Physiol.* 114:93–124 (published erratum appears in *J. Gen. Physiol.* 1999. 114:337).

Rothberg, B.S., and K.L. Magleby. 2000. Voltage and Ca2+ activation of single large-conductance Ca2+-activated K+ channels described by a two-tiered allosteric gating mechanism. *J. Gen. Physiol.* 116:75–99.

Sah, P.E., and M. McLachlan. 1992. Potassium currents contributing to action potential repolarization and the afterhyperpolarization in rat vagal motoneurons. *J. Neurophysiol.* 68:1834–1841.

Schreiber, M., and L. Salkoff. 1997. A novel calcium-sensing domain in the BK channel. *Biophys. J.* 73:1355–1363.

Schreiber, M., A. Yuan, and L. Salkoff. 1999. Transplantable sites confer calcium sensitivity to BK channels. *Nat. Neurosci.* 2:416–421.

Semenov, I., B. Wang, J.T. Herlihy, and R. Brenner. 2006. BK channel beta1-subunit regulation of calcium handling and constriction in tracheal smooth muscle. *Am. J. Physiol. Lung Cell. Mol. Physiol.* 291:L802–L810.

Shi, J., G. Krishnamoorthy, Y. Yang, L. Hu, N. Chaturvedi, D. Harilal, J. Qin, and J. Cui. 2002. Mechanism of magnesium activation of calcium-activated potassium channels. *Nature.* 418:876–880.

Stefani, E., M. Ottolia, F. Noceti, R. Olcese, M. Wallner, R. Latorre, and L. Toro. 1997. Voltage-controlled gating in a large conductance Ca2+-sensitive K+channel (hslo). *Proc. Natl. Acad. Sci. USA.* 94:5427–5431.

Storm, J.F. 1987. Action potential repolarization and a fast after-hyperpolarization in rat hippocampal pyramidal cells. *J. Physiol.* 385:733–759.

Wang, Z., W.O. Saifee, M.L. Nonet, and L. Salkoff. 2001. SLO-1 potassium channels control quantal content of neurotransmitter release at the C. elegans neuromuscular junction. *Neuron.* 32:867–881.

Wei, A., C. Solaro, C. Lingle, and L. Salkoff. 1994. Calcium sensitivity of BK-type K_{Ca} channels determined by a separable domain. *Neuron.* 13:671–681.

Xia, X.M., X. Zeng, and C.J. Lingle. 2002. Multiple regulatory sites in large-conductance calcium-activated potassium channels. *Nature.* 418:880–884.

Yang, X.C., and F. Sachs. 1989. Block of stretch-activated ion channels in Xenopus oocytes by gadolinium and calcium ions. *Science.* 243:1068–1071.

Zeng, X.H., X.M. Xia, and C.J. Lingle. 2005. Divalent cation sensitivity of BK channel activation supports the existence of three distinct binding sites. *J. Gen. Physiol.* 125:273–286.